

# Tunable photo-galvanic effect on topological insulator surfaces via proximity interactions

Yuriy G. Semenov, Xiaodong Li, and Ki Wook Kim\*

*Department of Electrical and Computer Engineering,  
North Carolina State University, Raleigh, NC 27695-7911*

## Abstract

An unusual photo-galvanic effect is predicted on the topological insulator surface when its semi-metallic electronic spectrum is modified by an adjacent ferromagnet. The effect is correlated with light absorption in a wide frequency range (from a few to hundreds of meV) and produces a pronounced response that is not only resonant to the photon energy but also tunable by an external electrical bias. The exceptionally strong peak photocurrent of the order of  $\mu\text{A}/\text{cm}$  may be achieved at elevated temperatures with the illumination power of  $1 \text{ W}/\text{cm}^2$  in the THz range on  $\text{Bi}_2\text{Se}_3$ . These advantages could enable room-temperature detection of far-infrared radiation.

PACS numbers: 72.40.+w, 72.25.Fe, 78.68.+m, 72.80.Tm

To date the photo-galvanic effect (PGE), i.e., direct current generation via light absorption in a structure with broken inversion symmetry, has been used as a unique experimental tool to study kinetic phenomena. Three different mechanisms are known to trigger the PGE: (i) the drag of electron gas by photons,<sup>1,2</sup> (ii) the imbalance in the excitation of electrons with opposite momenta,<sup>3,4</sup> and (iii) the shear of electron non-equilibrium distribution in the momentum space in the course of relaxation to equilibrium.<sup>3,5</sup> In this regard, the spin-orbit interaction leads to a specific manifestation of the latter two cases as it has been demonstrated previously that the transfer of optical spin polarization can realize a direct current.<sup>3</sup> However, the induced current is generally of low density due to the secondary role of spin-orbit coupling in the formation of band structure. Other approaches of PGE invariably suffer from the same fate of feeble response.

One potential exception may be the topological insulators (TIs) – the material with spin-orbit interaction so strong that it inverts the conduction and valence bands and exhibits numerous unusual phenomena deviating from the conventional perception about the magneto-electric effects.<sup>6–10</sup> It is plausible to expect the peculiar properties of TI surface states also modify the PGE, particularly when the time-reversal symmetry is broken by external fields. For instance, absorption of circularly polarized light was recently shown to generate a direct current in the surficial region of the TI.<sup>11</sup> Generally, this *circular* PGE is conditioned by the spin-momentum interlocked nature of the TI surface states. To get a nonzero response, however, a magnetic field  $B$  must break the three-fold rotational symmetry that results in an extremely weak photocurrent of  $\sim 10$  fA/cm under the excitation power of  $1$  W/cm<sup>2</sup> and  $B = 10$  T. A more pronounced effect ( $\sim 10$  nA/cm at  $T = 15$  K) was reported in Ref. 12, where the TI surface isotropy is broken by the obliquely incident light with an excitation energy much higher than the TI band gap. While the spin-orbit interaction is the key to the circular PGE, the weak low-symmetry interactions limit the density of dc transport to a low level in both cases as before.

In this study we draw attention to another, much stronger mechanism of PGE that stems from the band structure asymmetry at the interface between a TI and a proximate *insulating* or *dielectric* ferromagnet (FM). The basic principle of this effect is illustrated in Fig. 1. Here, the FM is assumed to be magnetized along the  $y$  axis that results in the shift of the TI surface Dirac cones along the  $x$  direction away from the  $\Gamma$  point in the momentum (i.e.,  $k$ ) space.<sup>9,10</sup> We focus, however, on one consequence of this shift beyond the contact

point that is manifested in the contortion of the conic shapes due to the spin-independent, quadratic-in- $k$  term [see the dashed curves in Figs. 1(b) and 1(c)]. Specifically, the states on the right side of the shifted Dirac cones in the figure are farther from the  $\Gamma$  point, in which the  $k^2$  term in the Hamiltonian increases more rapidly for both conduction and valence bands. For the n-type TI plotted in Fig. 1(b), the optical excitation is suppressed for the states on the left side of the Dirac cone, since both initial and final states are situated below the electrochemical potential  $\mu$ . On the other hand, the right side of the cone allows the transitions between resonant states via the same photons because they (i.e., the electronic states) are located astride  $\mu$ . Consequently, a significant imbalance induced in the momentum (i.e., group velocity) distribution of the excited electron ensemble produces a net photocurrent. Similarly, the p-type TI [Fig. 1(c)] gives a nonzero photocurrent along the opposite direction because the optical excitations on the right of the Dirac cones are suppressed instead.

As a didactic but practically important example of the approach, we start with a discussion on optical absorption in the TI/FM heterostructure before proceeding to the PGE. The corresponding states are described by the effective Hamiltonian of the low-energy TI surface electrons in an exchange interaction with a proximate magnet. Keeping the linear and quadratic terms of the two-dimensional electron momentum  $\mathbf{k} = (k_x, k_y, 0)$ , the Hamiltonian takes the form<sup>13</sup>

$$H = \hbar v_F [\vec{\sigma} \times \mathbf{k}] \cdot \hat{\mathbf{z}} + Dk^2 + \mathbf{G} \cdot \vec{\sigma}, \quad (1)$$

where  $\hat{\mathbf{z}} = (0, 0, 1)$  is the unit vector normal to the TI surface,  $v_F$  is the Fermi velocity,  $\vec{\sigma} = (\sigma_x, \sigma_y, \sigma_z)$  is the vector Pauli matrices of the electron spin, and  $D$  is the material parameter for the quadratic term. The last term in Eq. (1) describes the exchange interaction with the FM in terms of the effective exchange field  $\mathbf{G} = \xi \mathbf{M}$ , where  $\mathbf{M}$  denotes the FM magnetization and  $\xi$  is proportional to the exchange integral.<sup>14,15</sup> Since the exchange energy involves only the electron spin operators, its effect can be simply regarded as a momentum renormalization for the first term in Eq. (1), with  $k_y \rightarrow k_y + G_x/\hbar v_F$  and  $k_x \rightarrow k_x - G_y/\hbar v_F$ . In the case of  $\mathbf{M}$  directed along the  $y$  axis (i.e.,  $G_y = G$ ), the eigen-energies of the Hamiltonian are

$$\varepsilon_{b,\mathbf{p}} = dp^2 \pm \sqrt{(p_x - G)^2 + p_y^2}, \quad (2)$$

where  $\mathbf{p} = \hbar v_F \mathbf{k}$  is the momentum (in energy representation) of the conduction ( $b = c$ ) and valence ( $b = v$ ) electrons and  $d = D/\hbar^2 v_F^2$ . Note that the contact point energy corresponds

to  $\varepsilon_{c,\mathbf{p}} = \varepsilon_{v,\mathbf{p}} = dG^2$  due to the quadratic term. Accordingly, the relations  $\varepsilon_{c,\mathbf{p}} \geq dG^2$  and  $\varepsilon_{v,\mathbf{p}} \leq dG^2$  are satisfied by the conduction and valence bands, respectively. The reference (i.e., zero) of energy is defined at the Dirac point of unmodified TI surface states.

Let us consider a normally incident electro-magnetic wave whose electrical component  $\mathbf{E}$  generates the electric dipolar transitions. The case of monochromatic wave  $\mathbf{E} = E_0 \hat{\mathbf{e}} \exp[i(\mathbf{q} \cdot \mathbf{r} - \omega t)]$  corresponds to a certain polarization, where  $\omega$  is the angular frequency and  $\mathbf{q} = q\hat{\mathbf{z}}$  is the photon wave vector. The circularly polarized wave is described by polarization vector  $\hat{\mathbf{e}} = \hat{\mathbf{e}}_{\pm} = (\hat{\mathbf{x}} \pm i\hat{\mathbf{y}})/\sqrt{2}$ , while  $\hat{\mathbf{e}}_{\theta} = (\hat{\mathbf{x}} \cos \theta + \hat{\mathbf{y}} \sin \theta)$  corresponds to linear polarization with the angle  $\theta$  between the polarization plane and the  $x$  axis. The effect of unpolarized light can be described as a half sum of the contributions induced by non-coherent waves with perpendicular linear polarizations or opposite circular polarizations.

In the Coulomb gauge, the vector potential for the electro-magnetic radiation has the form  $\mathbf{A} = \text{Re}(i c \mathbf{E} / \omega)$ , where  $c$  is the velocity of light. From the perturbation treatment, the Hamiltonian of electron interaction with the radiation is

$$V = \frac{ev_F}{c} [\vec{\sigma} \times \mathbf{A}] \cdot \hat{\mathbf{z}} + \frac{2eD}{\hbar c} \mathbf{k} \cdot \mathbf{A}, \quad (3)$$

where  $e$  is the electron charge. Neglecting the small term containing  $D$ , the squared absolute value of electron-photon matrix element is given as  $|M|^2 = v_F^2 e^2 E_0^2 / 8\omega^2$  for both  $\hat{\mathbf{e}}_+$  and  $\hat{\mathbf{e}}_-$  polarization.<sup>16</sup> Thus, this is also applicable to unpolarized light. The effect of linear polarization appears in  $|M|^2$  as the additional factor  $2 \sin^2(\varphi_p - \theta)$  ( $\varphi_p$  is the angle between  $\mathbf{p}$  and  $\hat{\mathbf{x}}$ ), which reduces to 1 after averaging over  $\theta$ . An important property of the matrix element  $M$  is its independence on the electron momentum and exchange interaction.

The rate of photon energy absorption  $P = \hbar\omega \sum_{\mathbf{p}} (W_{v,\mathbf{p};c,\mathbf{p}} - W_{c,\mathbf{p};v,\mathbf{p}})$  is associated with the probability of interband transition  $|b, \mathbf{p}\rangle \rightarrow |b', \mathbf{p}\rangle$ :

$$W_{b,\mathbf{p};b',\mathbf{p}} = \frac{2\pi}{\hbar} |M|^2 f_0(\varepsilon_{b,\mathbf{p}}, \mu) [1 - f_0(\varepsilon_{b',\mathbf{p}}, \mu)] \delta(|\varepsilon_{b',\mathbf{p}} - \varepsilon_{b,\mathbf{p}}| - \hbar\omega). \quad (4)$$

Here we ignore the small photon momentum  $\mathbf{q}$  compared to  $\mathbf{k}$  as well as a minor deviation of the population factor  $f(v, \mathbf{p})$  from the equilibrium Fermi-Dirac function  $f_0(\varepsilon_{v,\mathbf{p}}, \mu)$ . Applying Eq. (2) to Eq. (4), straightforward integration of  $W_{v,\mathbf{p};c,\mathbf{p}} - W_{c,\mathbf{p};v,\mathbf{p}}$  over  $\mathbf{p}$  expresses the absorption rate  $P$  in terms of the roots of the energy  $\delta$  function  $p_x = p_{\lambda} \equiv G \pm \sqrt{(\hbar\omega/2)^2 - p_y^2}$

( $\lambda = \pm$ ) as well as the residual integral over  $p_y$ :

$$P(\hbar\omega, \mu) = \frac{\alpha}{8} P_i \int_{-\hbar\omega/2}^{\hbar\omega/2} \sum_{\lambda} \frac{f_0(\varepsilon_{v,\mathbf{p}\lambda}, \mu) - f_0(\varepsilon_{c,\mathbf{p}\lambda}, \mu)}{\sqrt{(\hbar\omega/2)^2 - p_y^2}} dp_y, \quad (5)$$

where  $\alpha = e^2/\hbar c$  is the fine-structure constant and  $P_i = (c/8\pi)E_0^2$  is the energy flow of the incident light. This equation allows simplification under the assumption of relatively small energy shift  $dG^2$  compared to the thermal energy  $k_B T$ . The final output in the normalized form (i.e., *normalized absorption*) can be written as

$$\frac{P(\hbar\omega, \mu)}{P_i} = \frac{\pi\alpha}{4} F(\nu, \eta); \quad F(\nu, \eta) = \frac{\sinh \nu}{\cosh \eta + \cosh \nu}, \quad (6)$$

in terms of arguments  $\nu = \hbar\omega/2k_B T$  and  $\eta = (4\mu - d\hbar^2\omega^2)/4k_B T$ . The factor  $\frac{1}{4}\pi\alpha F(\nu, \eta)$  determines the absorption ratio. At low temperature ( $\nu \gg 1$ ) in the absence of band curvature ( $d = 0$ ), this value is four times smaller than the graphene absorbance  $\pi\alpha \approx 2.3\%$ ,<sup>16</sup> reflecting the absence of degeneracy on valleys and spins. It is also obvious that  $\pi\alpha/4$  is the maximal structure absorbance attainable with a small  $|\mu|$  and high photon energy.<sup>17</sup>

Extending the analysis to the PGE begins with the general expression for the surface current in the diffusive regime

$$j = -\frac{e}{A_0} \sum_{b,\mathbf{p}} f(b, \mathbf{p}) v_x(b, \mathbf{p}), \quad (7)$$

where the axis  $x$  is directed along the electron flow,  $A_0$  is the area of the TI/FM interface, and  $\mathbf{v}(b, \mathbf{p}) = v_F \nabla_{\mathbf{p}} \varepsilon_{b,\mathbf{p}}$  is the electron group velocity. The electron distribution function  $f(b, \mathbf{p})$  contains the non-equilibrium effect due to light absorption [i.e., Eq. (4)]. When  $f(b, \mathbf{p}) = f_0(\varepsilon_{b,\mathbf{p}}, \mu)$  (i.e., in equilibrium), the current  $j$  becomes zero exactly. This also means the absence of dark current independent of the energy band distortions. Accordingly, we hereinafter focus on the deviation from the equilibrium distribution; i.e.,  $\Delta f(b, \mathbf{p}) = f(b, \mathbf{p}) - f_0(\varepsilon_{b,\mathbf{p}}, \mu)$ .

In the stationary case, the relaxation time approximation can yield a simple solution to the kinetic equation for the distribution function as  $\Delta f(b, \mathbf{p}) = S(b, \mathbf{p})\tau(b, \mathbf{p})$ , where  $\tau(b, \mathbf{p})$  is the relaxation time and  $S(b, \mathbf{p})$  is the rate of electron generation in the state  $|b, \mathbf{p}\rangle$ . In turn, the generation rate can be expressed via the probability of transitions discussed earlier [see Eq. (4)]; i.e.,  $S(b, \mathbf{p}) = \sum_{b'} (W_{b',\mathbf{p};b,\mathbf{p}} - W_{b,\mathbf{p};b',\mathbf{p}})$ . To extract the explicit effect of excitation imbalance in the electrons with opposite group velocities, it is sufficiently to restrict the

consideration to a constant relaxation time  $\tau(b, \mathbf{p}) = \tau$  independent of momentum  $\mathbf{p}$  and energy band  $b$ .<sup>11</sup> As such, the population imbalance is solely defined by photo-transition rates  $S(b, \mathbf{p})$ . At a fixed  $p_y$  and the photon energy  $\hbar\omega$  ( $> 2|p_y|$ ), the only states with  $p_x = p_{\pm}$  are involved in the interband transitions, while the proximity effect produces the energy difference  $\varepsilon_{b, \mathbf{p}_+} - \varepsilon_{b, \mathbf{p}_-} = 4dG\sqrt{(\hbar\omega/2)^2 - p_y^2}$  for both electron and valence bands (Fig. 1). This asymmetry between  $\varepsilon_{b, \mathbf{p}_+}$  and  $\varepsilon_{b, \mathbf{p}_-}$  presents the main reason for direct photocurrent generation. Indeed, it can be shown after some algebra that the summation over  $p_x$  in Eq. (7) produces an expression determined by the difference of the population factor rather than the velocities of photo-generated electrons and holes. The net photocurrent effect gives the integral over  $p_y$  for a given  $\hbar\omega$  provided that  $|\Delta f(b, \mathbf{p})| \ll f_0(\varepsilon_{b, \mathbf{p}}, \mu)$ :

$$j = \frac{\tau e}{2\pi\hbar^3 v_F} |M|^2 \int_{-\hbar\omega/2}^{\hbar\omega/2} dp_y \{ [f_0(\varepsilon_{v, \mathbf{p}_+}, \mu) - f_0(\varepsilon_{v, \mathbf{p}_-}, \mu)] - [f_0(\varepsilon_{c, \mathbf{p}_+}, \mu) - f_0(\varepsilon_{c, \mathbf{p}_-}, \mu)] \}. \quad (8)$$

Along with numerical evaluation, an analytical approximation of  $j$  would be desirable for a qualitative analysis of the effect. Assuming that the temperature is not too low ( $k_B T > dG^2$ ), Eq. (8) can be represented in terms of the incident light power and function  $F$ :

$$j = -\frac{\pi\alpha}{4} dG \frac{e v_F \tau}{k_B T} P_i F(\nu, \eta) F(\eta, \nu), \quad (9)$$

which explicitly displays the dependence of the PGE on absorption [Eq. (6)]. This expression clearly illustrates that the photocurrent originates from both the proximity effect ( $\sim G$ ), which breaks the isotropy of the interface Hamiltonian, and the spin independent parabolicity ( $\sim d$ ) of the energy bands. Furthermore, the dependence on photon energy (i.e., dimensionless variable  $\nu$ ) manifests a well-defined maximum that can be tuned by a change in the chemical potential. Note that switching in the FM magnetization ( $\mathbf{G} \rightarrow -\mathbf{G}$ ) leads to reversal of the photocurrent, which is in accordance with time-reversal symmetry inherent in the linear PGE.<sup>3</sup>

The photocurrent calculated in the structure with a typical TI is shown in Fig. 2 for different excitation energies at 300 K and 4 K. Specifically,  $\text{Bi}_2\text{Se}_3$  is assumed along with  $\tau = 1$  ps,  $G = 40$  meV, and the incident radiation power density of  $P_i = 1$  W/cm<sup>2</sup>. The maximum current density at room temperature is of the order of 0.1  $\mu\text{A}/\text{cm}$ , whereas it reaches over 10  $\mu\text{A}/\text{cm}$  at liquid helium temperature. These numbers are drastically

larger than the photocurrent reported earlier in TIs.<sup>11,12</sup> Another remarkable property of the proposed PGE is its correlation with the normalized absorption curves. As shown in Figs. 2(a) and 2(b), stronger and broader absorption characteristics leads to a similar trend in the photocurrent response at room temperature. On the other hand, the sharp transitions in the absorption curves (vs.  $\mu$ ) at low temperatures lead to the corresponding resonant current peaks [see Figs. 2(c) and 2(d)]. This can be understood clearly from Figs. 1(b) and 1(c); note also the relation  $\partial P/\partial\eta \propto j$  from Eqs. (6) and (9) although its validity is limited at low temperatures.

As indicated earlier, the main contribution to the photocurrent comes from the asymmetrical distribution of the photo-excited carriers that is in turn due to the shift  $G$  of the Dirac cones and the  $Dk^2$  term in the Hamiltonian. While the parabolicity is proportional to the parameter  $D$ , which is well-known for most TIs, the magnitude of the exchange energy may vary depending on the TI/FM materials as well as the quality of the interface. Based on the earlier studies in the literature,<sup>7,18–20</sup> it appears that  $G = 5 - 50$  meV can be expected. In the limit of low  $G$ , Eq. (9) predicts proportionality of the PGE to  $G$ . However, numerical evaluation of the more general expression [Eq. (8)] illustrates a saturating trend in the peak magnitudes of resonant curves  $j(\mu)$  as  $G$  increases ( $dG^2 \gg k_B T$ ). This is clearly visible in Fig. 3(a), where increasing  $G$  from 5 meV to 40 meV at  $T = 4$  K significantly broadens the resonant photo-response but introduces only a minor change in the peak height. The saturating behavior can be explained, at least in part, by the corresponding photon absorption curves. As can be seen from Fig. 3(b), an increase in  $G$  leads to a more gradual change in  $P$  with a decreased slope. Since both factors (i.e.,  $G$  and  $\partial P/\partial\eta$ ) contribute, their impacts compensate each other and the peak current remains largely unaffected.

Figure 3(c) shows the position (in  $\mu$ ) of the peak current as a function of the photon energy. The observed dependence is nearly linear in a wide range of photon energy, suggesting the equivalence (or strong correlation) between the frequency scanning and the chemical potential (thus, gate bias) sweeping in the detection of the PGE. In other words, the energy of incoming photons can be determined by measuring the TI surface current as a function of the gate bias. The strength of the photo-response is particularly pronounced at low temperatures as shown in Fig. 3(d). Note that all curves are calculated assuming an identical relaxation time  $\tau = 1$  ps. As the relaxation rate tends to decrease rapidly with temperature, further enhancement of PGE beyond tens of  $\mu\text{A}\cdot\text{cm}/\text{W}$  appears likely at  $T = 4$  K. Moreover,

the relaxation time can be much longer than 1 ps even at room temperature as the sample quality improves.

The strong PGE discussed above can be used to realize a photo-detector in the THz/far-infrared frequencies. One clear advantage of this mechanism is that the dark current can be eliminated without sacrificing the response time since the resulting photocurrent does not require an external bias. In conventional photo-detectors (such as those based on p-n junction photodiodes, Schottky barriers, quantum well structures, etc.), an external bias is applied to accelerate the excited carriers or to decrease the pn junction capacitance for fast response. However, the consequential dark current is detrimental to the device performance at room temperature as it is a powerful source of noise. The prospective device, on the other hand, is expected to work at room temperature with an extraordinary sensitivity, while having a very short response time. Since no junction is formed in the channel, the response time is determined by the carrier transit time. Not only the excited carriers have a high initial ensemble velocity ( $\sim v_F$ ) similar to the Schottky-barrier detector, but also the momentum relaxation in ideal TI surface states is expected to be very long, particularly for low energy electrons, due to the suppression of backscattering. Overall, the structure offers a unique opportunity for room-temperature detection of long-wavelength photons.

In summary, a linear PGE on the topological insulator (TI) surface adjacent to an insulating FM is examined. The dc photo-excitation stems from the TI surface band modification under the influence of both the symmetry-breaking proximate exchange interaction and spin-independent parabolicity of the dispersion law. The phenomenon is invariant to the sign of light circular polarization, thus effective at unpolarized excitation. At the same time, the PGE reveals the frequency-dependent resonance-like features, particularly for low temperatures, despite the absence of any discrete energy levels. The strong correlation between the excitation energy and photo-response enables straightforward detection of radiation frequency via electrical means such as the gate bias.<sup>21</sup> The photocurrent estimated with a relatively short relaxation time of 1 ps exceeds those of the previously reported PGEs by orders of magnitude. The proposed TI/FM structures may have significant advantages over the conventional devices in the detection of long-wavelength photons beyond the thermal noise limit.<sup>22,23</sup>

This work was supported, in part, by the SRC Focus Center on Functional Engineered Nano Architectonics (FENA) and the US Army Research Office.



---

\* Electronic address: kwk@ncsu.edu

- <sup>1</sup> A. M. Danishevskii, A. A. Kastal'skii, S. M. Ryvkin, and I. D. Yaroshetskii, *Sov. Phys. JETP* **31**, 292 (1970).
- <sup>2</sup> K. Zeeger, *Semiconductor Physics* (Springer, New York, 1973), Chap. 11.
- <sup>3</sup> E. L. Ivchenko and G. E. Pikus, *Superlattices and Other Heterostructures* (Springer, Berlin, 1995).
- <sup>4</sup> H. Diehl, V. A. Shalygin, L. E. Golub, S. A. Tarasenko, S. N. Danilov, V. V. Bel'kov, E. G. Novik, H. Buhmann, C. Brüne, L. W. Molenkamp, E. L. Ivchenko, and S. D. Ganichev, *Phys. Rev. B* **80**, 075311 (2009).
- <sup>5</sup> E. L. Ivchenko and S. D. Ganichev, in *Spin Physics in Semiconductors*, ed. M. I. Dyakonov (Springer, Berlin, 2008), p. 245.
- <sup>6</sup> H. Zhang, C. X. Liu, X. L. Qi, X. Dai, Z. Fang, and S. C. Zhang, *Nature Phys.* **5**, 438 (2009).
- <sup>7</sup> W.-K. Tse and A. H. MacDonald, *Phys. Rev. Lett* **105**, 057401 (2010).
- <sup>8</sup> W. Zhang, R. Yu, H. J. Zhang, X. Dai, and Z. Fang, *New J. Phys.* **12**, 065013 (2010).
- <sup>9</sup> M. Z. Hasan and C. L. Kane, *Rev. Mod. Phys.* **82**, 3045 (2010).
- <sup>10</sup> X. L. Qi and S. C. Zhang, *Rev. Mod. Phys.* **83**, 1057 (2011).
- <sup>11</sup> P. Hosur, *Phys. Rev. B* **83**, 035309 (2011).
- <sup>12</sup> J. W. McIver, D. Hsieh, H. Steinberg, P. Jarillo-Herrero, and N. Gedik, *Nat. Nanotechnol.* **7**, 96 (2012).
- <sup>13</sup> W. Y. Shan, H. Z. Lu, and S. Q. Shen, *New J. Phys.* **12**, 043048 (2010).
- <sup>14</sup> B. D. Kong, Y. G. Semenov, C. M. Krowne, and K. W. Kim, *Appl. Phys. Lett.* **98** 243112 (2011).
- <sup>15</sup> T. Yokoyama, Y. Tanaka, and N. Nagaosa, *Phys. Rev. B* **81**, 121401(R) (2010).
- <sup>16</sup> R. R. Nair, P. Blake, A. N. Grigorenko, K. S. Novoselov, T. J. Booth, T. Stauber, N. M. R. Peres, and A. K. Geim, *Science* **320**, 1308 (2008).
- <sup>17</sup> X. Zhang, J. Wang, and S. C. Zhang, *Phys. Rev. B* **82**, 245107 (2010).
- <sup>18</sup> Y. G. Semenov, J. M. Zavada, and K. W. Kim, *Phys. Rev. B* **77**, 235415 (2008).
- <sup>19</sup> H. Haugen, D. Huertas-Hernando, and A. Brataas, *Phys. Rev. B* **77**, 115406 (2008).
- <sup>20</sup> J. Chakhalian, J. W. Freeland, G. Srajer, J. Stremper, G. Khaliullin, J. C. Cezar, T. Charlton,

R. Dalgliesh, C. Bernhard, G. Cristiani, H.-U. Habermeier, and B. Keimer, *Nature Phys.* **2**, 244 (2006).

<sup>21</sup> J. Chen, H. J. Qin, F. Yang, J. Liu, T. Guan, F. M. Qu, G. H. Zhang, J. R. Shi, X. C. Xie, C. L. Yang, K. H. Wu, Y. Q. Li, and L. Lu, *Phys. Rev. Lett.* **105**, 176602 (2010).

<sup>22</sup> S. P. Apell, G. W. Hanson, and C. Hägglund, arXiv:1201.3071v1.

<sup>23</sup> S. Thongrattanasiri, F. H. L. Koppens, and F. Javier García de Abajo, *Phys. Rev. Lett.* **108**, 047401 (2012).

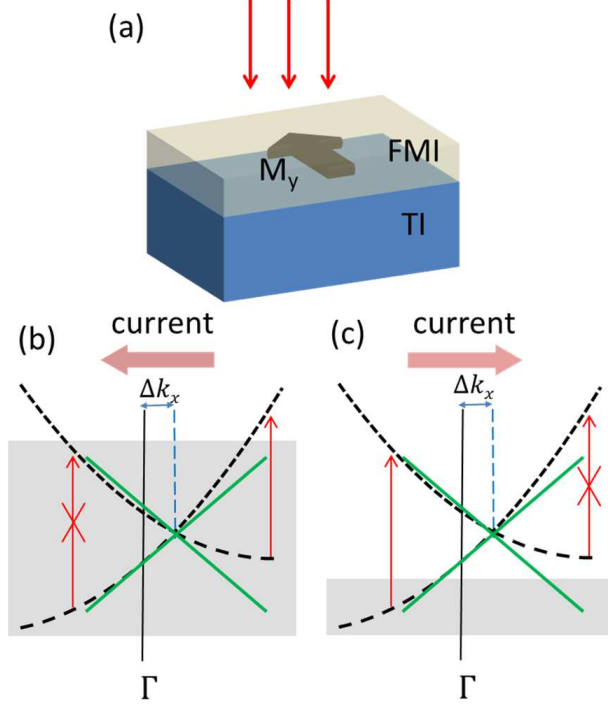


FIG. 1: (Color online) Schematic illustration of photocurrent generation on a TI surface adjacent to an insulating ferromagnet (FM). (a) TI/FM hybrid device structure. The arrows indicate the incident electro-magnetic radiation and the block arrow denotes the magnetization of the FM layer. (b,c) Photocurrent generation in a n-type TI and a p-type TI, respectively. The dashed lines are the TI surface bands taking into account the  $k^2$  term and the proximity effect, while the solid lines only include the proximity effect. The shaded area denotes the filled states under electrochemical potential  $\mu$ .

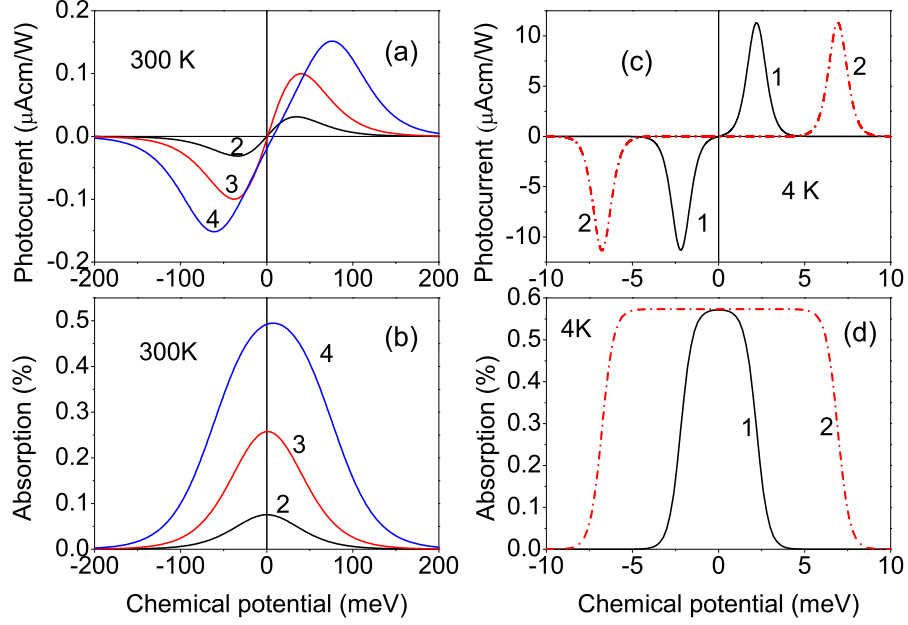


FIG. 2: (Color online) Photocurrent density and normalized absorption curves at (a,b) 300 K and (c,d) 4 K versus the chemical potential with different excitation energies:<sup>4</sup>  $\hbar\omega = 4.4$  meV, 13.7 meV, 50 meV, and 135 meV for curves 1, 2, 3 and 4, respectively. All calculations assume the relaxation time  $\tau$  of 1 ps and the proximate exchange energy  $G$  of 40 meV along with the material parameters corresponding to  $\text{Bi}_2\text{Se}_3$  ( $v_F = 4.28 \times 10^7$  cm/s and  $D = 13$  eV $\cdot\text{\AA}^2$ ).

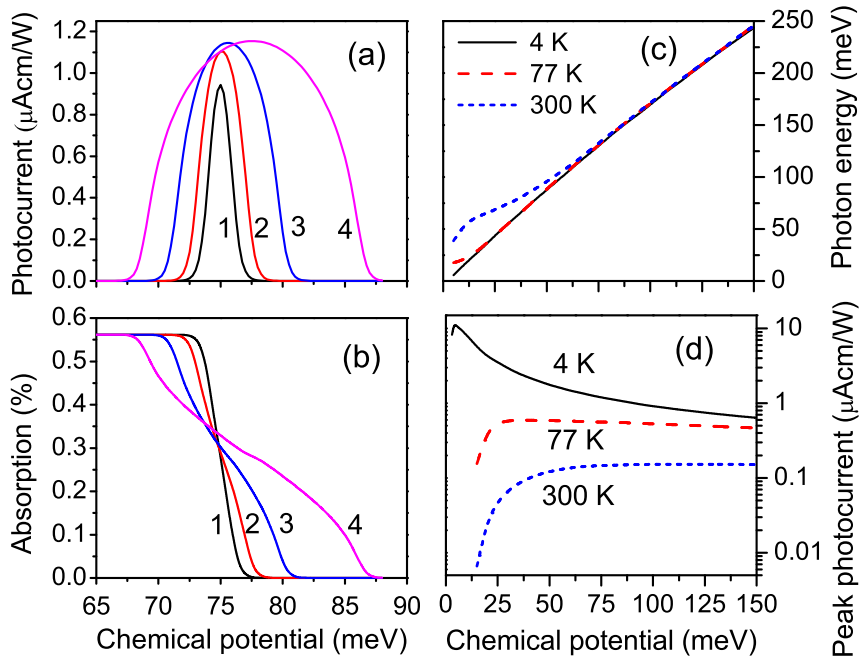


FIG. 3: (Color online) (a) Resonance-like photocurrent and (b) normalized absorption curves at 4 K with the excitation energy of 135 meV. Curves 1, 2, 3, and 4 represent the results with the proximate exchange energy  $G$  of 5 meV, 10 meV, 20 meV, and 40 meV, respectively. (c) Photon energy vs. peak position in the chemical potential  $\mu$  and (d) corresponding peak photocurrent at different temperatures.  $G = 40$  meV is used for (c) and (d).